The effect of stress-dependent SWRC on the load carrying capacity of the slope subjected to the drying-wetting path

Chidanand M Jadar[1*], *Sathiyamoorthy* Rajesh[2], and *Suman* Roy[3]

[1]Reseach Scholar, Department of Civil Engineering, IIT Kanpur, Uttar Pradesh, India, 208016
[2]Professor, Department of Civil Engineering, IIT Kanpur, Uttar Pradesh, India
[3]Assistant Professor, Department of Civil Engineering, GITAM School of Technology, GITAM University, Bengaluru, Karnataka, India, 562163

Abstract. The stability and load capacity of structures resting on compacted soil slopes is one of the major concerns in Geotechnical Engineering practice. The mechanically compacted earthen slopes are prone to the dynamic exchange of flux flow, resulting in varying saturation levels across their entire configuration. The soil water retention curve (SWRC) is a property which significantly controls the stability and load capacity of structures resting on these compacted soil slopes. The parameters of a typical SWRC are affected by net stress and climatic changes in field conditions, adding more complexity in evaluating the load capacity and stability of structures resting on these compacted soil slopes. To analyze this issue critically, the load capacity of a footing resting on an unsaturated compacted soil slope under year-long arid climatic conditions has been evaluated numerically in the present study. The effect of net stress has been considered by assessing the stress-dependent SWRC of chosen soil under the wetting and drying cycle at various net confinements of 10 kPa, 100 kPa, and 200 kPa in the laboratory. Key parameters of the SWRCs under drying and wetting cycles were incorporated to evaluate the load capacity of the footing resting on the unsaturated soil slope.

1 Introduction

In recent years, globalization, urbanization, and overpopulation are compelling people to construct various structures in non-conventional spaces. These structures are significantly affected by the surrounding environments, imposing a threat to their durability and stability. A typical example of such structures is buildings on hilly terrains. These hilly terrains constitute compacted soil slopes under exposed climatic conditions, leading to varying saturation levels throughout the year. The groundwater table fluctuation also contributes to the variation in the pore water pressure distribution across the vadose zone. In such cases, the load capacity of the structures resting on these compacted soil slopes varies significantly throughout the year. Further, imposed loads on these slopes due to the construction of these structures add more complexity to the analysis [1].

Determination of the load capacity of these structures resting on compacted unsaturated soil slopes requires a comprehensive transient state analysis [2]. During the transient analysis, the nature of the soil water retention curve (SWRC) of the chosen soil should be carefully adopted as the key parameters of the SWRC are significantly affected by the stress state and corresponding wet-dry cycles [3,4]. Over the past few years, various researchers have tried to determine the load capacity of structures resting on these typical unsaturated soil slopes utilizing different numerical methodologies [5]. The importance of considering SWRC in these analyses has also been explored by researchers [6]. Recently, the load capacity of footings resting on expansive unsaturated soils was also determined using a novel limit equilibrium technique. Considering the literature review mentioned above, it can be acknowledged that various researchers have probed into the mechanism of determination of load carrying capacity of footing resting on the unsaturated slopes efficiently. However, the effect of considering SWRCC coupled with drying-wetting cycles has not been addressed properly by researchers.

Therefore, the present work focuses on utilizing a combination of SWRC and drying-wetting cycles to determine the load capacity of a footing resting on a homogeneous unsaturated compacted soil slope at different times of the year. The geometry of the homogeneous unsaturated compacted soil slope was adopted from the literature, while the compacted soil was an expansive artificial bentonite sand mix chosen by the authors. An in-depth parametric numerical study is done utilizing a commercially finite element software SVOffice to get the load-carrying capacity of the footing resting on the unsaturated slope at a different time of the year. A comprehensive justification on the need of considering the theories of unsaturated soil mechanics is concluded along with the results.

* Corresponding author: cmjadar@iitk.ac.in

2 Material Properties

The chosen soil in the present study is 80S20B soil, a mixture of commercially available powdered sodium bentonite, 80% by weight, and Kalpi sand, 20% by weight. The sand was obtained from the Kalpi site and was dried, passed through 425 μm, and retained on 212μm before mixing with dry powdered bentonite.

Index properties of the chosen soil were determined according to ASTM D4318-17 [7]. The liquid and plastic limits of the 80S02B soil were 84.3% and 28.45%, respectively. Also, a maximum dry density (γ_{dmax}) of 15.99 kN/m^3 and optimum moisture content (OMC) of 18.25% were observed for 80S20B soil.

2.1 Determination of stress-dependent SWRC in the volumetric plane under the drying-wetting cycle

Soil water retention curve (SWRC) is a unique property of unsaturated soils that relates the water content (gravimetric/volumetric) or the degree of saturation with the soil suction. In the present study, the stress-dependent SWRC of 80S20B soil was determined under drying and wetting cycles. The axis translation technique is the most favoured method for determining the SWRC of soil under drying and wetting cycles. However, the axis translation technique may not be suitable for expansive soils because of the high air entry value and high suction levels in these soils. Due to these constraints associated with the axis translation technique, an indirect method [8] to measure SDSWRC of 80S20B soil under drying and wetting cycles was adopted in the present study.

The compacted 80S20B soils at predetermined density and molding water content were consolidated in an oedometer at the desired net stress levels. Further, the suction and the volumetric deformations of these compressed samples along both drying and wetting paths were determined to obtain the volumetric SWRC of 80S20B soil. Details of this procedure are explained in the subsequent paragraphs.

2.1.1 Oedometric Compression

For the oedometeric compression experiment, three identical samples of 80S20B soil were compacted at a predetermined density and molding water content (γ, 16.25 kN/m^3 and w, 20.25%) in a compaction ring using the static compaction technique. After the preparation of the compacted samples, they were saturated under seating loads (5 kPa) in the oedometer apparatus. The oedometer apparatus was filled with water, and the compacted samples were gradually allowed to saturate and swell, during which the volume change was continuously monitored through the dial gauge readings. Upon noticing no deviations in the dial gauge readings for three consecutive days, specific loads were imposed on the samples. One of the samples had a 0 kPa load to simulate the null stress condition. In contrast, the other two samples were set with a vertical load of 150 kPa (equivalent to net mean stress of 100 kPa considering a K_0 value of 0.5) and 300 kPa (equivalent to net mean stress of 200 kPa considering a K_0 value of 0.5) to simulate isotropic confinement of 100 kPa and 200 kPa respectively. The samples were allowed to consolidate under these imposed loads.

2.1.2 SWRC Determination

At the end of primary consolidation, the compacted samples were carefully removed from the oedometer ring. Shelby tube samplers of 38 mm diameter were driven into the oedometer samples, and WP4C specimens were gradually extracted, as shown in the inset of Figure 1. For the drying SWRC, these specimens were air dried intermittently at different water contents, and the suction at these specific water contents was measured using a dew-point potentiameter. After the complete air-drying phase, the samples were oven dried at a temperature of 70°C. As the bentonite content was 20%, it did not exhibit any major cracks on the surface. For the wetting SWRC, these oven-dried samples were wetted to different water contents by sprinkling water from the top and were stored in an air-tight closed chamber for 24 hours to ensure uniform suction equilibration. The suction values at these specific water contents using a dew point potentiameter (WP4C). Thus, a drying and wetting stress-dependent SWRC of 80S20B soil was obtained in the gravimetric plane.

The volumetric deformation of 80S20B soil during the drying-wetting cycles under net stress was also monitored in the present study. The samples were pre-consolidated and extracted using a 50 mm Shelby tube similar to the SWRC samples. These samples were further trimmed to fit in a shrinkage dish of 50 mm diameter and dried intermittently. The shrinkage samples were weighed at each drying stage, and the deformation was measured using vernier calipers. On the completion of the drying phase, the samples were wetted intermittently, similar to the drying stage. For each wetting stage, the weight and the deformation of the compacted sample were measured. The relationship between the void ratio and gravimetric water content obtained from the shrinkage curves was utilized to determine the volumetric SWRC of 80S20B soil at various net stresses. Further, these volumetric SWRC of 80S20B soil at different net stress was fitted with the Fredlund and Xing (1994) [10] model, as shown in Figure 1 and the fitting parameters for all these fits are presented in Table 1

Table 1. Fitting parameters of SWRC

	Net stress (kPa)	a (kPa)	m	n	R^2
Drying	10	685.74	1.246	0.885	0.999
	100	798.79	0.582	1.967	0.998
	200	880.93	0.620	1.984	0.998
Wetting	10	186.05	0.915	1.175	0.994
	100	383.06	0.562	1.873	0.998
	200	466.78	0.420	2.547	0.943

It should be noted that Even though the data points are close, slight differences in the water content can lead to huge changes in suction values, as the suction values are on a logarithmic scale. Therefore, this would substantially affect the numerical analysis. So, they cannot be treated uniquely.

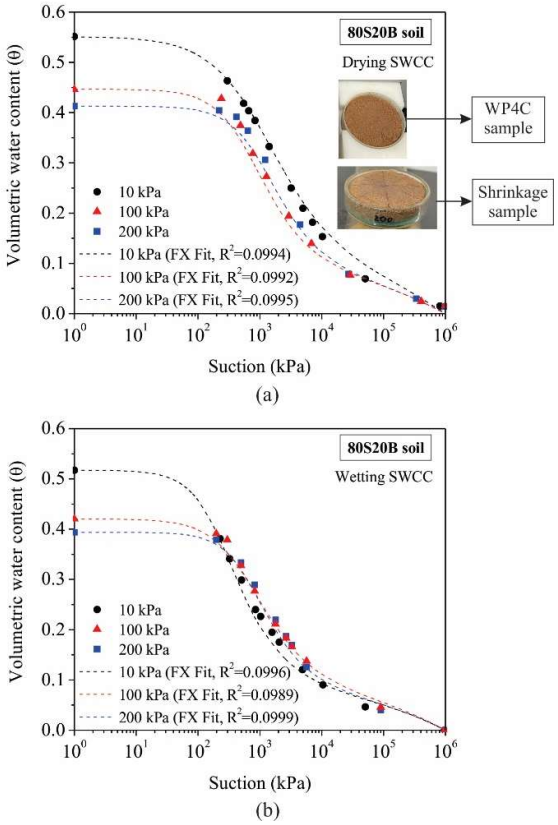

Fig. 1. Stress-dependent SWRC in (a) drying path (inset showing dew point potentiameter and shrinkage samples extracted from oedometer samples) and (b) wetting path

3 Numerical Modelling and Analysis

For the numerical modeling, a homogeneous slope was adopted from the literature [9]. The homogeneous slope was modeled in SVOffice, a commercially available FEM-based numerical software. The analysis was carried out by coupling the flux modules and the slope module of the FEM-based numerical software. Details regarding the modeling are explained in the subsequent sections.

3.1 Hydraulic behaviour analysis

3.1.1 Numerical modelling of the of the problem

The geometry of the slope, adopted from [9], is presented in Figure 2 (a). The sloping portion of the homogeneous slope has a 10m height and a slope angle of 26.6°, as shown in Figure 2 (a). The initial location of the water table is at a depth of 5m below the sloping portion's toe.

To account for the effect of stress-dependent SWRC on the homogeneous slope, the entire slope was divided into three zones (top, middle, and bottom), considering the magnitude of vertical stress distribution as shown in Figure 2 (b). The unsaturated properties of 80S20B soil at the top zone of the slope were assumed to be governed by the SWRC of 0/10 kPa. On the other hand, the unsaturated properties of 80S20B soil at the middle and the bottom zone of the slope were governed by 100 kPa and 200 kPa SWRC, respectively. Corresponding hydraulic conductivity functions of the respective SWRC derived using Fredlund and Xing's (1994) [10] permeability function were also provided as input in the respective zones of the numerical model.

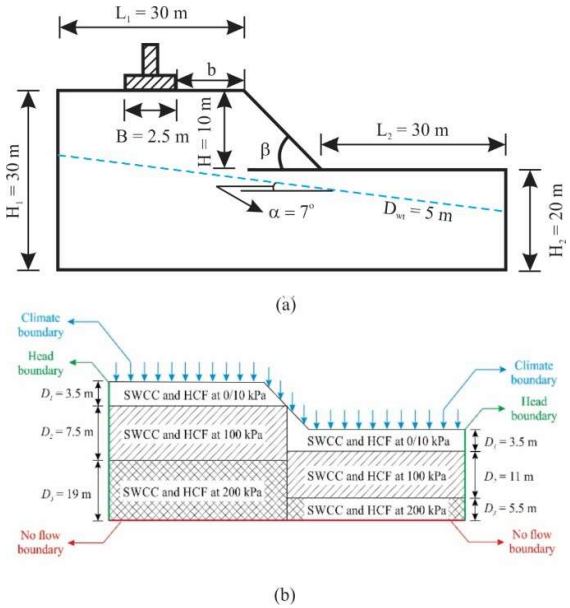

Fig.2. The geometry of the homogenous slope with footing dimensions

SVOffice employs Richard's equation to analyze the flow in the unsaturated zone. FlexPDE algorithm solves the combined governing partial differential equation (PDE) for two-dimensional transient saturated/unsaturated considering liquid water and water vapor fluxes. Richard's equation can be given as,

$$\frac{\partial}{\partial x}\left(k_{wx}\frac{\partial h}{\partial x}+k_{vd}\frac{\partial u_w}{\partial x}\right)+\frac{\partial}{\partial y}\left(k_{wy}\frac{\partial h}{\partial y}+k_{vd}\frac{\partial u_w}{\partial y}\right)=\gamma_w m_2^w\frac{\partial h}{\partial t} \quad (1)$$

where x and y are the coordinates in the horizontal and vertical directions, k_{wx} and k_{wy} are the hydraulic conductivity functions in the horizontal and vertical directions, k_{vd} is the vapor conductivity, u_w is the pore-water pressure and m_2^w is the derivative of SWRC with respect to suction.

The initial pore water distribution was obtained by running a steady-state analysis with a nominal flux of 0.00001m/day at the ground surface. After the steady-state analysis, the transient analysis was carried out utilizing the pore water pressure conditions obtained at the end of the steady-state analysis. The relevant boundary conditions for the transient state analysis are shown in Figure 2 (b). A climatic condition corresponding to an arid zone (Kanpur) was also provided as an input for climatic conditions in the

transient state analysis. The details of the climatic conditions are shown in Figure 3. It should be noted that, as the slope was subjected to a broad distribution of drying and wetting seasons, corresponding drying/wetting stress-dependent SWRCs were fed in the model depending on the particular climatic boundary conditions. Stress-dependent wetting SWRC was utilized for rainy seasons, while stress-dependent drying SWRC was used for other seasons. Automatic time stepping and adaptive grid refinement was employed in the numerical model. The finite element order was set to quadratic. An initial time increment of 0.2 days and a maximum increment time of 0.3 days were given in the formulations. The error limit was kept to 0.002 for the finite element analysis.

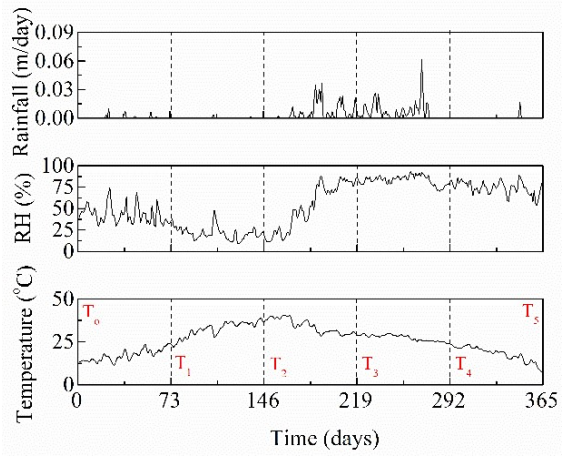

Fig.3. Daily average precipitation, Relative humidity, and average daily air temperature of Kanpur for the year 2019 (Jan-Dec)

3.1.2 Volumetric water content and suction behaviour

The volumetric water content and suction distribution at various time intervals over the entire year were obtained by transient analysis. Two monitoring sections, AA' and BB, were chosen to monitor this. Section AA´ was at the crest of the sloping section, while BB´ was at the toe of the sloping section. The properties were observed at five different periods throughout the year at an interval of 73 days, as shown in Figure 3.

Fluctuations in the volumetric water content (VWC) over 365 days are shown in Figure 4. It was evident that the VWC increased during the rainy season. Similar to VWC profiles, suction profiles over the influence of yearlong climatic conditions are shown in Figure 5.

It is observed from Figures 4 and 5 that the profiles of VWC and suction varied significantly along the entire length of the monitoring sections throughout the year. The suction varied from 0 kPa to 18000 kPa at section AA´, while at BB´, it varied from 3 kPa to 12000 kPa (for the 146th day of the dry season). For volumetric water content, both sections experienced a variation from 0.1 to 0.55 (for the 146th day of the dry season), respectively. The suction decreased considerably in the interval between 146th day and to 219th day. This fall in the suction can be attributed to the heavy precipitation during the rainy season.

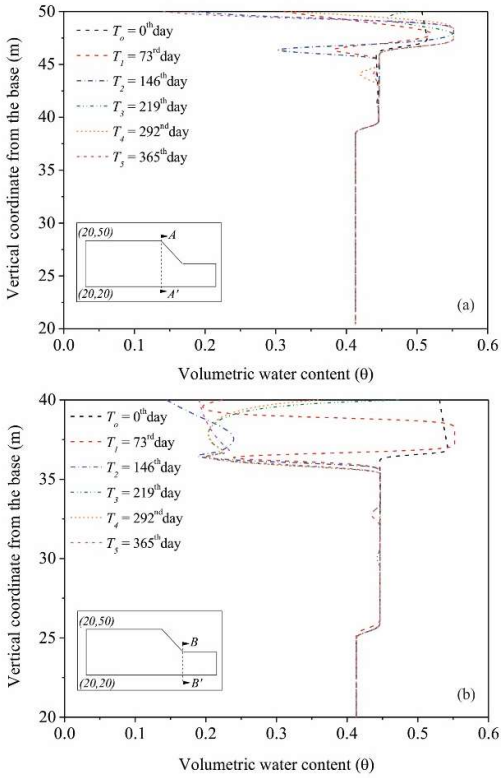

Fig.4. Vertical profile of VWC (a) at the crest (b) at the toe

3.2 Load-carrying capacity analysis

3.2.1 Methodology for determining the load-carrying capacity

Post assessment of the hydraulic behavior of the homogeneous slope, the load-carrying capacity of a strip footing resting on the homogeneous slope was determined. A footing resting on a homogeneous soil slope can be considered a conventional slope stability problem or a bearing capacity problem Both assessments can effectively provide the maximum load capacity of the footing resting on the homogeneous soil slope. However, the analysis principle is typically different for each of these methods. For a slope stability analysis, the load on the footing is gradually incremented, and the slope's safety factor concerning shear strength in peak or critical state is noted. On the other hand, for bearing capacity analysis, the rate of loading and displacements are controlled to determine the load capacity of the footing at peak loading or a predetermined displacement. Therefore, both of these methods may evaluate a different load capacity for the same problem. In the present study, as strength is the most important aspect, the load capacity of the footing is determined using conventional slope stability methodology.

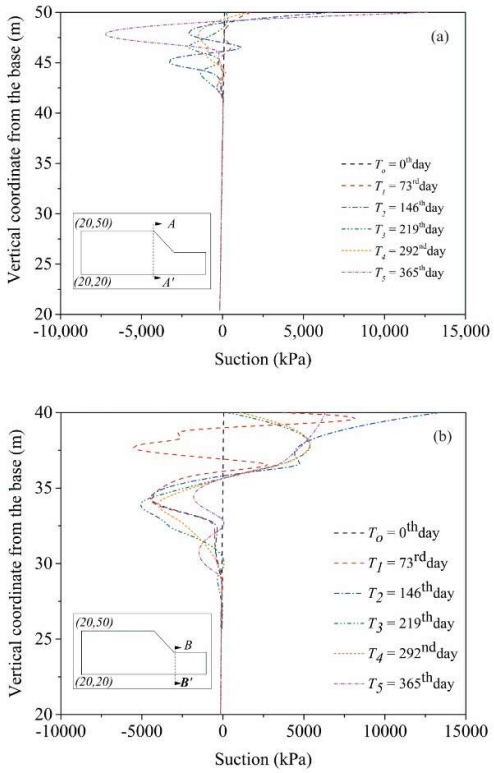

Fig.5. Vertical profile of suction (a) at the crest (b) at the toe

3.2.2 Numerical modeling of the problem

The load capacity of the footing resting at the edge of the homogeneous slope was determined from the slope stability analysis in SVOffice.

In the slope stability analysis, the hydraulic behavior of the homogeneous slope at different times of the year was used as an input to analyze the factor of safety (FOS) of the slope using the limit equilibrium method. The drained shear strength parameters of the 80S20B soil were determined experimentally. The saturated cohesion intercept, c' of 80S20B soil, was observed to be 12 kPa, while the effective friction angle ϕ' was observed to be 35°. From the SVSlope module, the unsaturated Vanapalli et al. (1994) model was utilized to predict the unsaturated shear strength of 80S20B soil over the entire suction range. The strip footing at the slope's edge was assumed to be 2.5m wide.

The load on the footing was sequentially increased from 0 to 1000 kPa at an interval of 200 kPa, and the factor of safety at each load was determined by slope stability analysis. A critical FOS of less than one, as per Eurocode 7 (2004), was considered to determine the ultimate load capacity of the footing. The variation of FOS at different times of the year for each load increment is presented in Figure 6. At the beginning of the year, under the influence of small precipitation, the FOS slightly decreases on the 73rd day. However, with the onset of the summer season, the relative humidity (RH) decreases, and the temperature also increases between the 73rd and 146th day, causing an increase in the FOS. During the post-summer season, the region experienced heavy precipitation. With the rise in the volumetric water content, the suction decreased significantly. As a result, a significant decrement in the magnitude of FOS was noticed at the end of the 219th day. The rainy season continued till the 292nd day. During this period, the ultimate load capacity of the footing of 183 kPa is observed, corresponding to a FOS of 1. After this period, a dry period was observed till the end of the year (365th day), during which the FOS increased.

A comparison of the observed load capacity of the footing at the edge of the homogeneous slope with drying-wetting cycles and SWRC is also made with the conventional analysis. The conventional analysis considers load capacity of the footing resting on the edge of the slope without the utilization of drying-wetting cycles and SWRC. In this case, it is observed that the ultimate load of the footing is never reached in this typical analysis. In addition, a comparison of the observed load capacity of the footing at the edge of the homogeneous slope with drying-wetting cycles and SWRC is also made with the load capacity of the footing resting on the edge of the saturated slope. It is observed that a slightly lower load capacity of 158 kPa is predicted by considering the full saturated slope in analysis.

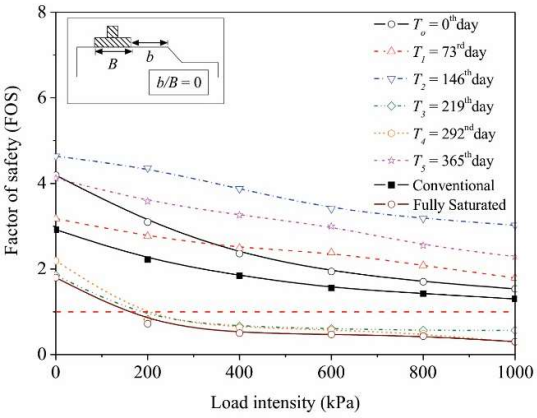

Fig.6. Stability chart for footing at the edge of a homogeneous slope considering climatic conditions and SWRC

4 Load carrying capacity of the footing

A detailed parametric study was carried out to evaluate the variation in the load-carrying capacity of the footing resting on the top of the homogeneous slope with the distance from the edge of the slope. The parametric study was characterized by three different methods. Initially, the slope was analyzed using the conventional slope stability method without utilizing the SWRC and the climatic conditions. In the conventional method, soil properties were taken according to hydrostatic flow conditions. Above the groundwater table, the bulk unit weight and below, the saturated unit weights were considered. A critical slope stability condition was considered in the second method, where the soil in the entire slope was taken as saturated. In the third method, the slope was analyzed, accounting for the SWRC and the climate variations. The parametric study was considered by varying the *b/B* ratio, where *B* is the width

of the footing and *b* is the distance between the right end of the footing and the crest of the slope. Figure 7 shows the variation in FOS and the loading capacity with the distance of footing from the edge of the slope. It was observed that with the increase in the distance from the edge of the slope, the ultimate loading capacity of the footing increased (403 kPa for *b/B* = 1, 590 kPa for *b/B* = 2, 680 kPa for *b/B* = 3). Also, considering the SWRC and climatic variations, the ultimate loading capacity was more compared to the saturated conditions (almost 16% to 43% increase in loading capacity compared to saturated conditions) and less compared to the conventional method analysis (the ultimate load capacity is not reached in the conventional analysis as the FOS is always greater than 1).

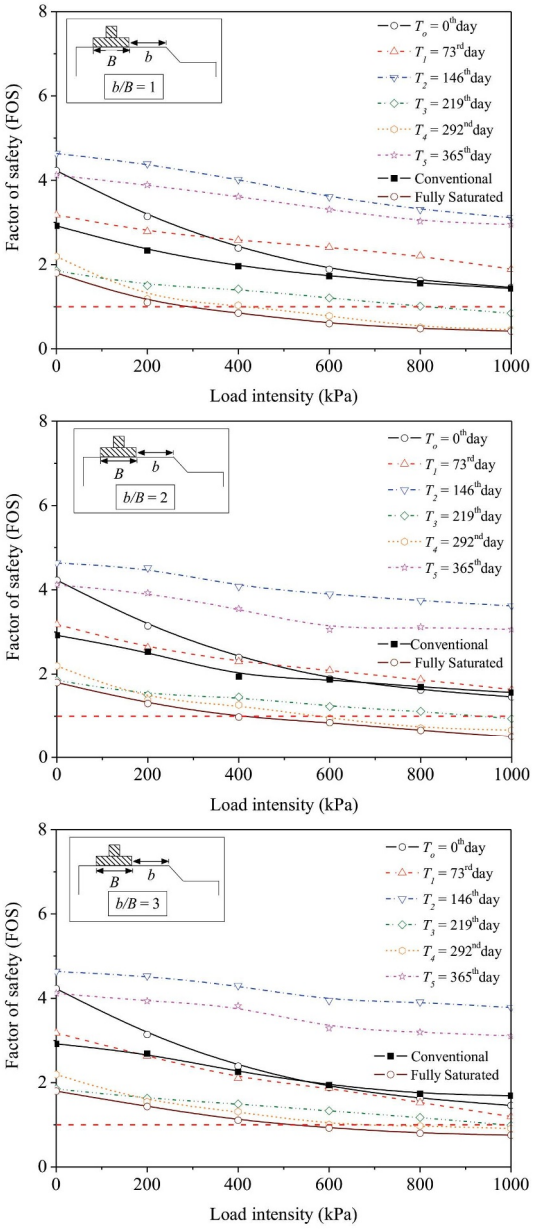

Fig.7. Variation of FOS at different b/B ratio

The above discussion on load capacity infers that with the increase in the distance of the footing from the edge of the slope, a fully saturated analysis significantly underestimates the ultimate load capacity. In contrast, the conventional analysis significantly overestimates the ultimate load capacity of the footing. Even during the rainy season, the ultimate load capacity of the footing using SWRC and climatic variations is almost 30% to 43% more than the results obtained using saturated analysis. Thus the unsaturated zone below the footing significantly affects the analysis and the economy considering the structure. The considered factor of safety associated with the ultimate load capacity of footings can be lowered for design considerations.

5 Conclusions

The study involved the determination of the ultimate load capacity of a footing resting on the top of a homogenous slope of 80S20B soil through numerical modelling. Based on the present analysis following points can be presented:

- The saturated volumetric water content decreases with the increase in net stress and with the advent of the wetting cycle in the volumetric SWRC of 80S20B soil. Also, the air entry value decreases with the increase in net stress.
- The ultimate load capacity of the footing is higher in unsaturated real field conditions of the slope when compared to the saturated conditions. The ultimate load capacity, in this case, is almost 16% to 43% more than in saturated conditions.
- Considering conventional conditions of the slope, the ultimate load capacity of the footing is significantly higher than the ultimate load capacity obtained by using unsaturated real field conditions of the slope.
- With the increase in the distance from the edge of the slope, the ultimate load capacity of the footing increases gradually.

References

1. L. Plantedis, D. V. Griffiths, Eng. Geol. Soc. Territ. **2**, 1231–1234. (2015)
2. N. Gofar, and H. Rahardjo, MATEC Web of Conferences, 05004 (2017)
3. S. Roy, S. Rajesh, Int. J. of Geomechs. **20(3)**, (2020)
4. H. Rahardjo, T. T. Lim, M. F. Chang, D. G. Fredlund, Can. Geotech. J. **32**, 60-77 (1995)
5. W. T. Oh, S. K. Vanapalli, Can. Geotech. J**. 48**, 425-438 (2011)
6. C. W. W. Ng, Y. W. Pang, J. Geotech. and Geoenv. Eng.**126 (2)**,157-166 (2000)
7. ASTM D4318-17e1ASTM Intl.
8. C.W.W. Ng, Pang, Can. Geotech. J. **37**, 1252-1264 (2000)
9. H. Rahardjo, T. H. Ong, R. B. Rajaur, E. C. Leong, J. Geotech. and Geoenv. Eng.**133(12)**, 1532–1543 (2007)
10. D. G. Fredlund, A. Xing, Can. Geotech. J. **31**, 533–546. (1994)